Study of the interaction between a Mn ore and alkali chlorides in chemical looping combustion

Daofeng Mei [a,*], Anders Lyngfelt [a], Henrik Leion [b], Tobias Mattisson [a]

[a] *Division of Energy Technology, Department of Space, Earth and Environment, Chalmers University of Technology, Chalmersplatsen 4, Gothenburg, Sweden*
[b] *Department of Chemistry and Chemical Engineering, Chalmers University of Technology, Chalmersplatsen 4, Gothenburg, Sweden*

ARTICLE INFO

ABSTRACT

Chemical looping combustion (CLC) is a novel technology for heat and power generation with inherent CO_2 capture. Using biomass in CLC (bio-CLC), negative CO_2 emissions can be attained. Biomass usually contains high content of alkalis (mainly K and Na) which can be problematic in the process, such as potential alkali-bed interaction, and this is the focus of current work. This work uses charcoal with and without the impregnation with alkali chlorides, KCl and NaCl. The results are compared to previous data from samples impregnated with K_2CO_3 and Na_2CO_3. A low-alkali braunite manganese ore is used as bed material to study the oxygen carrier interaction with the alkalis in cyclic experiments at 950 °C in a quartz batch fluidized-bed reactor. As compared to charcoal without alkali impregnation, the impregnation with KCl, NaCl, K_2CO_3, and Na_2CO_3 can improve the rate of gasification by a factor of 4, 3, 10, 8, respectively. Partial-defluidization of the braunite particles was found with all the alkali-fuels, although the extent differed, e.g., K_2CO_3 and KCl resulted in earlier onset of defluidization than Na_2CO_3 and NaCl. Further, indications of partial defluidization were earlier and more permanent with the carbonates than the chlorides. Partial agglomeration with soft agglomerates of the bed was observed, while hard agglomerations were never seen. Accumulation of K, Na, Si, and Ca was found in the agglomerates after cycles with K_2CO_3-charcoal and Na_2CO_3-charcoal, while little K and Na was detected in the bridges between particles after the KCl and NaCl cycles. A significant fraction of the alkali added was found in the oxygen carrier, with 80% or more being retained for the Na salts, and around 40% for the K salts. There was no clear difference between chlorides and carbonates with respect to retention. The fresh and used braunite have very similar reactivity with CH_4 and H_2, whereas some decrease in reactivity is noticed with CO.

1. Introduction

Although the concept of chemical looping combustion (CLC) was presented a long time ago in a patent for pure CO_2 generation [1], the development of this process, however, has mainly taken place in the last two decades, starting with the first demonstrations in CLC pilots for gaseous [2,3] and solid fuel [4,5]. The process uses a transition metal oxide (called oxygen carrier) to transfer the oxygen needed for fuel combustion [6]. The oxygen carrier provides oxygen for fuel combustion in the fuel reactor and then is re-oxidized in the air reactor [7]. Therefore, fuel in the CLC process never mixes with air, and this results in a flue gas stream with the product gases CO_2 and H_2O being undiluted by air-nitrogen. Thus, a stream of CO_2 can be realized through simple steam condensation and, ideally, no gas separation is needed to capture CO_2. Therefore, CO_2 capture in CLC has very low energy penalty. Many oxygen carriers have been tested in CLC systems [8,9] and these include synthesized materials, natural ores (iron ore, ilmenite, manganese ore, etc.) and industrial by-products (red mud, steel slag, etc.) [8]. Natural ores, have low costs and are widely studied in CLC [10]. Use of biomass in CLC (bio-CLC) can achieve negative CO_2 emissions, because the atmospheric CO_2 absorbed in biomass growth is captured in CLC, and thus CO_2 is removed from the atmosphere. Thus, bio-CLC could be important, considering the rapid exhaustion of the global carbon budget for 1.5/2°C temperature rise. Bio-CLC has been successfully operated in 0.5–100 kW_{th} pilot units [8,9,11–19] and partial bio-CLC has been tested in a 12 MW_{th} boiler [20].

Biomass in general has a high volatiles content, some char and a small content of ash-alkalis (e.g. 0.2% of the fuel weight) [21]. In large-scale bio-CLC systems, the biomass throughput can be 50 ton/h to maintain an aimed thermal power (e.g. 250 MW_{th}). Therefore, the

Table 1
Main components (weight percent) in the charcoal, alkali-fuels and minor metal elements in the braunite oxygen carrier. Data for K_2CO_3-fuel and Na_2CO_3-fuel are from previous work [28].

	Proximate (%, as received)				Ultimate (%, air dried)				Metals (%, air dried)				
	FC	V	M	A	C	H	N	S	Al	Si	Ca	Na	K
Charcoal	84.3	4.9	1.9	8.9	89	<0.3	0.5	0.7	1	2.7	0.1	0.03	0.05
K_2CO_3-fuel	53	15.7	3.3	28	73	<0.3	0.4	0.4	0.8	2	0.1	0.04	8.1
Na_2CO_3-fuel	62.2	14.7	3.1	20	80	<0.3	0.4	0.9	0.9	2.4	0.1	4.9	0.03
KCl-fuel	55.7	6.4	8.9	29	64	<0.5	0.3	0.5	0.6	1.6	0.1	0.04	5.2
NaCl-fuel	62.7	5.5	6.8	25	71	<0.5	0.4	0.3	0.8	2	0.1	5.2	0.03
Braunite									0.4	2.6	2.5	0.29	0.22

corresponding alkali input to the system can be as high as 100 kg/h, which can lead to various operation problems [22,23], including bed agglomeration, oxygen carrier reactivity decrease and fouling of steam tube surfaces [24,25]. These in turn can cause bad system performance and even failure of operation. Nevertheless, the unique two-reactor configuration in CLC could result in some advantages with high alkali fuels, as the fuels have less chance to contact with the heat-exchangers in CLC [26,27], thus lowering the risk of heat exchanger fouling. This is because in CLC most of the cooling is inside, and downstream of, the air reactor, whereas there are no cooling surfaces in the fuel reactor where alkalis are mainly released [26]. Nonetheless, the oxygen carrier bed in the fuel reactor has direct contact with alkalis, and this can lead to oxygen carrier and alkali interactions [28–31], which could be advantageous or disadvantageous for CLC operation [32,33]. Some studies suggest that the impregnation of K^+ or Na^+ can greatly enhance the conversion of CO to CO_2 with an ilmenite oxygen carrier [34]. But it seems the enhancement depends a lot on the type of alkali and oxygen carrier [35,36]. The fluidization and agglomeration behaviours of oxygen carriers in fluidized beds are other important aspects of the presence of alkali, as low-melting point alkali species could be formed and are generally considered responsible for agglomeration [31,35,37]. Alkali distribution in CLC system has been studied through gas-phase alkali measurement and solid-phase alkali characterization in experimental campaigns in a 60 kW$_{th}$ pilot and a 100 kW$_{th}$ CLC pilot [17–19,38]. The majority of alkali is retained in the oxygen carrier material, while some left the fuel reactor in gas-like form, and little was detected at the air reactor exit. The alkali retention in the bed may further lead to oxygen carrier reactivity change, cause unstable operation and even defluidize/agglomerate the bed [28,39]. Further studies are needed to understand the alkali-oxygen carrier interaction in bio-CLC process.

The objective of this work is to investigate the interaction of alkali with an oxygen carrier, and involved experiments with KCl and NaCl and a braunite manganese ore oxygen carrier as well as a comparison to previous work using alkali carbonates, K_2CO_3, Na_2CO_3 [28]. The experiments were performed in batch fluidized bed, and were designed to give a release of alkali similar to real conditions, i.e. from fuel particles located inside the fluidized bed. Given the practical limitations of performing a vast number of oxidation-reduction cycles, the experiments were also designed to give a high release of alkali in each cycle. For this purpose the two alkali salts were separately impregnated in charcoal particles which were used as fuel. More than 30 reduction-oxidation cycles with each alkali-fuel were conducted in the batch reactor. The purpose of the work was to see if the effects of alkali on oxygen carrier reactivity, on agglomeration tendency, as well other physical-chemical properties.

2. Experimental

2.1. Fuel and oxygen carrier

Methane, syngas (50 %CO + 50 %H$_2$), charcoal and charcoal samples impregnated with KCl, NaCl, were the fuels used, and results were compared to previous work with charcoal impregnated with K_2CO_3, and
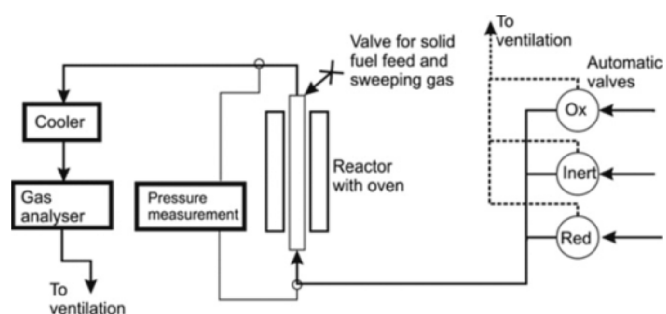

Fig. 1. Schematic description of the batch fluidized bed reactor system.

Na_2CO_3. The impregnated charcoals are named KCl-fuel, NaCl-fuel, K_2CO_3-fuel and Na_2CO_3-fuel. An incipient dry impregnation method was used for the alkali-charcoal preparation. Details of the impregnation method can be found in previous work [28]. In brief, a certain amount of alkali solution corresponding to the total pore volume of charcoal is introduced to the charcoal under stirring. The charcoal was then stirred and dried slowly to remove the water and thus an alkali containing charcoal was obtained. For some alkalis, successive impregnation was conducted to reach a certain alkali loading. Care was taken to avoid "overloading", i.e. to avoid any visible layer of salt on the outer surface. For this reason, the impregnated amount differs between the salts. As shown in Table 1, the charcoal before alkali impregnation contains 84.3% fixed carbon, 4.9% volatiles, 8.9% ash and 1.9% moisture, and the alkali content is negligible. The alkali impregnation resulted in 8.1 % K in the K_2CO_3-fuel, 4.9% Na in the Na_2CO_3-fuel, 5.2 % K in the KCl-fuel and 5.2% Na in the NaCl-fuel. This corresponds to 0.28 mol Na for Na_2CO_3, 0.33 mol K for K_2CO_3, 0.56 mol K for KCl and 0.54 mol Na for NaCl, i.e. per 100 g charcoal. There is also some silicon present in the five solid fuels. The oxygen carrier used is a manganese ore called braunite which has been studied in previous CLC pilot operations [28,38] and lab tests [40]. Before use, the braunite underwent a consecutive heat-treatment at 500 °C for 1 h and 950 °C for 12 h, and then was sieved to particles with diameter of 100–300 μm. The heat-treatment was conducted to strengthen the Mn particles and to remove moistures and volatiles, and to bring the materials on an equal level by starting from the same state of oxidation. The oxygen carrier has 52% Mn, 11% Fe and some additional compounds, shown in Table 1, and based on X-ray crystallography (XRD) characterization, braunite (Mn_7SiO_{12}) is the main phase in the heat-treated manganese ore.

2.2. Reactor setup and test procedure

A fluidized bed reactor with batch feeding of oxygen carrier and fuel was used to simulate the reduction and oxidation in CLC process [28,41,42]. The reactor tube is made from quartz and can be heated to 1000 °C with the surrounding oven. The reactor temperature is monitored with a K-type thermocouple which was protected with a quartz shell and inserted into the bed. As shown in Fig. 1, the reacting/fluidizing gas is controlled and switched with three automatic valves on the

Table 2
Series of cycles with CH$_4$ (◻), Charcoal (◻) and alkali-fuels (◻). Blank (□) means no experiment; Bold "m" indicates the middle cycle for bed material sampling; Syngas cycles are not shown here. The K$_2$CO$_3$ and Na$_2$CO$_3$ experiments were conducted in previous work [28].

Series	Cycle Number																			
Cycle 1-20	*1*	*2*	*3*	*4*	*5*	*6*	*7*	*8*	*9*	*10*	*11*	*12*	*13*	*14*	*15*	*16*	*17*	*18*	*19*	*20*
K$_2$CO$_3$	pink	pink	pink	pink	pink	pink	gray	gray	gray	green	green	green	green	green	green	green	**m**	gray	gray	gray
Na$_2$CO$_3$	pink	pink	pink	pink	pink	pink	green	green	green	green	green	green	green	green	green	**m**	gray	gray	gray	gray
KCl	pink	pink	pink	pink	pink	green	green	green	green	green	green	green	green	green	green	green	pink	pink	pink	pink
NaCl	pink	pink	pink	pink	pink	pink	pink	pink	pink	pink	pink	pink	pink	gray	gray	pink	pink	green	green	green
Cycle 21-40	*21*	*22*	*23*	*24*	*25*	*26*	*27*	*28*	*29*	*30*	*31*	*32*	*33*	*34*	*35*	*36*	*37*	*38*	*39*	*40*
K$_2$CO$_3$	pink	pink	pink	green	green	green	green	green	green	green	green	green	green	pink	pink	pink	pink	pink	gray	gray
Na$_2$CO$_3$	pink	pink	green	green	green	green	green	green	green	green	green	green	green	pink	pink	pink	pink	gray	gray	gray
KCl	green	green	green	green	green	green	green	green	green	green	green	green	green	**m**	green	pink	pink	green	green	green
NaCl	green	green	green	green	green	green	green	green	green	green	green	green	green	**m**	green	green	green	green	green	green
Cycle 41-60	*41*	*42*	*43*	*44*	*45*	*46*	*47*	*48*	*49*	*50*	*51*	*52*	*53*	*54*	*55*	*56*	*57*	*58*	*59*	*60*
K$_2$CO$_3$	gray	gray	pink	pink	pink	green	green	green	green	green	green	green								
Na$_2$CO$_3$	pink	pink	pink	pink	pink	green	green	green	green	green	green	green								
KCl	pink	pink	pink	pink																
NaCl	green	green	green	green	green	green	green	green	green	green	green	green	green	green	green	green	green	pink	pink	
Cycle 61-63	*61*	*62*	*63*																	
NaCl	pink	pink	pink																	

right-side. These valves switch the reacting environment among reduction, inert and oxidation, which are marked with "Red", "Inert" and "Ox" in the figure. In reduction, gaseous fuels (CH$_4$ and syngas) enter from the inlet at the bottom while the solid fuel was injected from the top valve with the help of a continuous sweeping N$_2$. A pressure transducer connecting the reactor top and bottom was used to measure the pressure-drop over the bed and to monitor the fluidization status. Downstream of the reactor is an electric cooler and a gas analyzer (Rosemount NGA2000). The cooler removes steam from the gas which is then sent to the analyzer. Concentrations of CH$_4$, CO, CO$_2$, H$_2$ and O$_2$, pressure signal and gas volumetric flow were sampled. All data were registered in a computer connected to a data logger.

In all the tests, the reactor temperature was set to 950 °C. All the oxidations were made with 5% O$_2$ atmosphere. In reduction with gaseous fuels, only the fuel gas (either CH$_4$ or syngas) was used. The fuel flow rate at the reactor inlet was kept at 345 ml/min for CH$_4$ and 450 ml/min for syngas, which corresponds to u_g/u_{mf} = 9 and 12. The bed was 20 g braunite in the case with CH$_4$. In the case with syngas, a mixture of 2 g braunite and 13 g sand was used as bed material to avoid full conversion of the syngas in order to provide the best data evaluation of reactivity [42]. In the solid fuel experiments, the gasification/fluidization gas was a mixture of 48% H$_2$O and 52 % N$_2$ with a total flow rate of 865 ml/min, and the gas flow corresponds to u_g = 0.4 m/s and u_g/u_{mf} = 31. In the reduction period with solid fuels, around 0.1 g fuel were injected from the reactor top with the help of N$_2$ sweeping in a flow of 300 ml/min. In total, 42–63 redox cycles for different alkali fuels were made and Table 2 shows the four series included in the comparison. In all cases, the oxygen carrier was first stabilized with CH$_4$ cycles and then used in solid fuel experiments. After the stabilization, several cycles with charcoal without alkali were conducted as reference, expect for the KCl series. Then, the oxygen carrier was exposed to numerous cycles with an alkali-fuel. The charcoal and alkali-fuel were used alternatively for several rounds. Solid samples were extracted from the middle cycles, as indicated with "m" in Table 2. These samples were denoted "K$_2$CO$_3$-middle", etc. Similarly, solid samples from the series end are denoted as "K$_2$CO$_3$-final", etc. The reactivity of these "middle" and "final" oxygen carrier samples was evaluated through the reactions with CH$_4$, while

their physical and chemical properties were analyzed. The reactivity of calcined and used braunite with syngas was also studied, but this is not under the series in Table 2 and thus is not shown in the table.

3. Data evaluation

3.1. Gaseous fuels

Mass-based oxygen carrier conversion, ω, was used to evaluate the extent of oxygen carrier reduction in the reduction period. The amount of weight loss from the oxygen carrier is equivalent to the amount that was consumed by the fuel during reduction. Thus, the oxygen carrier conversion with CH$_4$ and syngas can be calculated through Eqs. (1) and (2) below.

$$\omega_{CH_4} = 1 - \int_{t_0}^{t} \frac{\dot{n}_{out} M_O}{m_{ox}} (4x_{CO_2} + 3x_{CO} - x_{H_2}) dt \tag{1}$$

$$\omega_{syn} = 1 - \int_{t_0}^{t} \frac{\dot{n}_{out} M_O}{m_{ox}} (2x_{CO_2} + x_{CO} - x_{H_2}) dt \tag{2}$$

where $\dot{n}_{out}$ is the dry gas flow after the correction of a flowmeter value measured with the gas analyzer [28]. M_O is the atomic oxygen molar mass, m_{ox} represents the amount of oxygen carrier in the bed. The symbol x_i takes the concentration of gas i (i = CO$_2$, CO or H$_2$) at time t.

Gas yield, γ_i (i = CH$_4$ and CO or H$_2$), presents the extent of fuel conversion to CO$_2$ and H$_2$O. This parameter was calculated from gas concentrations at time t and reflects the oxygen transfer efficiency in the reduction period.

$$\gamma_{CH_4} = \frac{x_{CO_2}}{x_{CH_4} + x_{CO} + x_{CO_2}} \tag{3}$$

$$\gamma_{CO} = \frac{x_{CO_2}}{x_{CO} + x_{CO_2}} \tag{4}$$

$$\gamma_{H_2} = 1 - \frac{x_{H_2}}{x_{CO} + x_{CO_2}} \tag{5}$$

Table 3
Typical relative errors of different parameters.

ω_{CH4}, ω_{syn}, X_C	γ_{CH4}	γ_{CO}	γ_{H2}	r_{inst}
±3%	±8.6%	±1.7%	±0.4%	±6%

3.2. Solid fuels

The cumulative mass of carbon left the reactor at time t, $m_C(t)$, was obtained through Eq. (7) by integrating the carbonaceous gas flows (CH_4, CO_2 and CO).

$$m_C(t) = \int_{t_0}^{t} \dot{n}_{out} M_C (x_{CH_4} + x_{CO_2} + x_{CO}) dt \tag{6}$$

where M_C is the molar mass of atomic carbon. With $m_C(t)$, the charcoal conversion $X_C(t)$ was obtained as the ratio between $m_C(t)$ and the total carbon $m_{C,tot}$ calculated for the entire reduction.

$$X_C(t) = \frac{m_C(t)}{m_{C,tot}} \tag{7}$$

The char gasification rate r_{inst} was obtained through Eq. (8) which was formulated based on the residual carbon amount.

$$r_{inst} = \frac{1}{1 - X_C} \frac{dX_C}{dt} \tag{8}$$

3.3. Pressure fluctuation

To better identify the defluidization, the amplitude of pressure fluctuation, σ, was calculated through Eq. (9). Data from the middle part of the period of oxidation, to avoid influence of steam addition and gas switching, was used for the calculation. The data was broken into smaller groups of 9. This was found to be necessary to avoid drifts or stepwise variations in the average pressure to influence the calculated amplitude. Thus, the average of the data from these groups was used to calculate σ in Eq. (9).

$$\sigma = \frac{1}{N-m} \sum_{i}^{N-m} \left(\frac{1}{m} \bullet \sum_{j=i}^{i+m} (\Delta p_j - \Delta p_{avg})^2 \right)^{0.5} \tag{9}$$

where N is the number of pressure-drop values used for evaluation, m, the number of samples of each small group, is 9, and i is the ith pressure-drop, Δp_{avg} is the average of the m + 1 pressure-drop values and Δp_j is the jth pressure drop value.
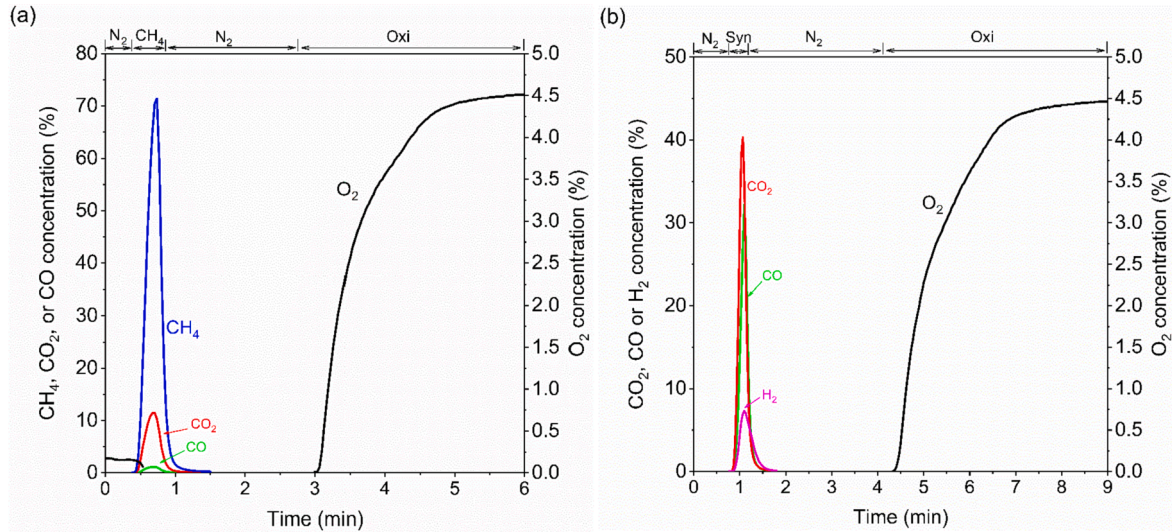

Fig. 2. Concentrations of CH_4, CO, CO_2, H_2 and O_2 as a function of time for a typical cycle of the fresh braunite oxygen carrier with (a) CH_4 and (b) syngas at 950 °C.
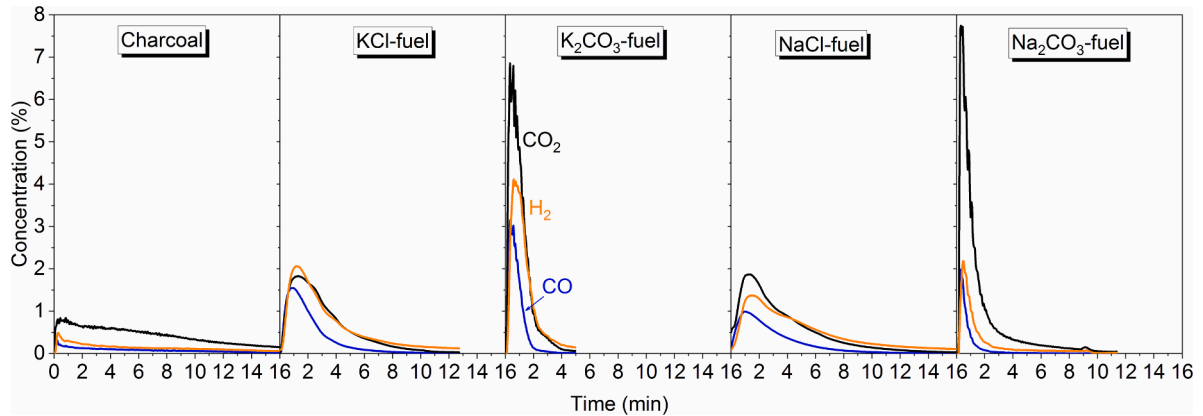

Fig. 3. Concentrations of CO, CO_2 and H_2 during the braunite reduction with Charcoal, KCl-fuel, K_2CO_3-fuel, NaCl-fuel and Na_2CO_3-fuel at 950 °C under the fluidization with 48% H_2O + 52 % N_2. Data for K_2CO_3 and Na_2CO_3 are from previous work [28].
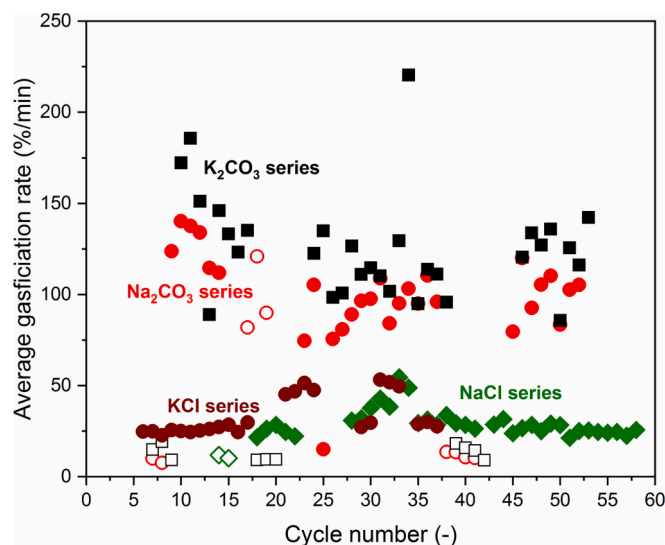
Fig. 4. Rate of char gasification as a function of cycle number during the reduction period of K_2CO_3 (■, □), KCl (●), Na_2CO_3 (●, ○) and NaCl (◆, ◇) series experiments. Void symbols are tests with Charcoal, the KCl series has no charcoal tests. K_2CO_3 and Na_2CO_3 data are derived from previous results [28].

3.4. Uncertainty analysis

All the parameters above were calculated based on the gas concentrations measured with the gas analyzer (NGA2000), thus the uncertainty of gas analysis will propagate to the final results. The measurement of CO, CO_2, CH_4, H_2 and O_2 with the NGA2000 analyzer has uncertainty of $\pm 1\%$. A formula, detailed in previous work [12] for uncertainty propagation estimation, is used to analyze the relative errors of the above parameters, and the uncertainties are summarized in Table 3 below. The uncertainty of final results is in the range of $\pm 0.4 - 8.6\%$. Among the parameters, γ_{H2} has the lowest error of $\pm 0.4\%$ and γ_{CH4} has the highest uncertainty of $\pm 8.6\%$.

4. Results and discussion

4.1. Typical cycles with CH_4 and syngas

Fig. 2 shows a typical cycle with CH_4 and syngas. The cycle is composed by consecutive periods of reduction marked with "CH_4" or "Syn", inert marked with "N_2" and oxidation marked with "Oxi". In the case of CH_4, more than 70% of the fuel remains unconverted and the

peak concentrations of CO_2 and CO are only 11.5% and 1.1%, indicating low reactivity of CH_4 with the braunite. Despite low conversion of CH_4 there was no carbon deposition, which would have been detected in the subsequent oxidation periods. The syngas, however, shows higher conversion of CO and H_2, despite much less oxygen carrier in the bed (2 g Mn ore and 13 g sand) in the syngas tests. Thus, <7% H_2 and <30% CO were seen after the reactor.

4.2. Typical reactions with solid fuels

A typical reduction period with Charcoal, KCl-charcoal, K_2CO_3-charcoal, NaCl-charcoal and Na_2CO_3-charcoal is shown in Fig. 3. In the case of Charcoal without alkali impregnation, the main gas product was CO_2 while the gasification intermediates (CO and H_2) were low. Thus, a major part of the CO and H_2 from the gasification reacted with the oxygen carrier and was oxidized to CO_2 and H_2O. CO_2, H_2 and CO were seen for a long time when using Charcoal, even after 15 min following the fuel feeding. When alkali-fuels were used, all gas concentrations were significantly higher than for Charcoal in first minutes, thus showing a faster gasification of the impregnated charcoals, as a consequence of the catalytic effects of K and Na [43,44]. In all the reduction cycles with charcoal and impregnated charcoal, H_2 is higher than CO although the latter generally is less reactive with the oxygen carrier. This is likely a result of the water-gas shift reaction, which converts CO and H_2O to CO_2 and H_2 under steam rich conditions.

4.3. Rate of gasification

The rate of char gasification was calculated through Eq. (8), and here the average value obtained in the range $X_C = 0.3–0.7$, is used for comparison, see Fig. 4. Clearly, the addition of alkalis in the charcoal promoted the gasification, as a result of the alkali catalytic effect. In the case of Charcoal without any alkali impregnation, the rate is around 10%/min. This was, however, increased to around 25–120%/min when KCl, NaCl, Na_2CO_3 and K_2CO_3 were added to charcoal. Among all the four alkalis, KCl and NaCl show distinctly lower gasification rates as compared to K_2CO_3 and Na_2CO_3. This is in line with previous works, where a range of potassium salts [45] and sodium salts [46] were compared for their catalytic activity on gasification. In the cases of K_2CO_3, Na_2CO_3 and NaCl series, Charcoal was regularly used after alkali fuels, and the results indicate that the previous use of alkali-charcoals has no obvious effects on the gasification rate of pure charcoal. Thus, the alkali that is retained in the oxygen carrier, as discussed in section 4.6 below, does not affect the char gasification.
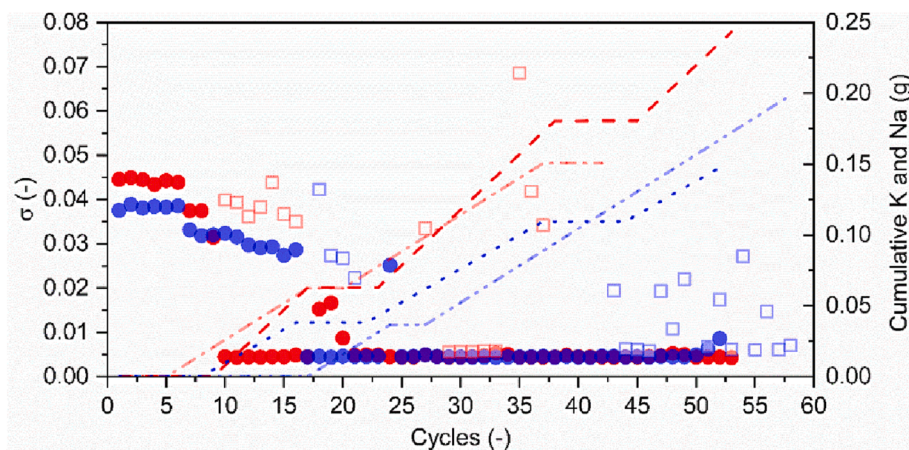

Fig. 5. Amplitude of pressure fluctuation in the KCl (□), K_2CO_3 (●) NaCl (□) and Na_2CO_3 (●) series of experiment, and the calculated cumulative amount of K from K_2CO_3 (- -) and KCl (-•-), NaCl (-••-) and Na_2CO_3 (• •) added in the cycles. K_2CO_3 and Na_2CO_3 data are from previous work [28].

Fig. 6. Partial agglomeration of the braunite oxygen carrier.

4.4. Partial defluidization

The pressure fluctuation σ for the four series of experiment is shown as a function of cycle number in Fig. 5. Some of the data in the KCl and NaCl series of studies are not available, because of some difficulties with the pressure transducer, whereas most of the data in K_2CO_3 and Na_2CO_3 series are available. In all cases fluctuation is high in the initial cycles, in the range 0.025–0.045, with some gradual decrease. The fluctuation with carbonates then dropped to a very low value (<0.005) and remained there for the rest of the cycles. This drop happened already in cycle 10 in the K_2CO_3-fuel series, and a bit later for the Na_2CO_3 series (cycle 17). The pressure fluctuations during the cycles with CH_4 in the KCl and NaCl series are not available, but they should be similar to those

in K_2CO_3 and Na_2CO_3 series. The KCl and NaCl series also showed a gradual decrease in fluctuation, indicating partial defluidization. But cycles with really low fluctuations came later for the chlorides. Although there are some cycles with very low fluctuations, e.g. 29–33 for KCl and 44–46 for NaCl, there are also later cycles with high fluctuations. In the case of KCl, this increase in fluctuations coincided with the cooling down and extrusion of the "middle" sample. Thus, the indications of partial defluidization in Fig. 5 appear both earlier and show more permanence for the carbonates, as compared to the chlorides. Alkali chlorides are known to be especially difficult in biomass combustion in terms of fouling, but perhaps the smaller effect can be explained by the KCl being more easily evaporated than K_2CO_3, NaCl and Na_2CO_3 [47,48]. Moreover, the equilibrium partial pressure of the reactions KCl ↔ KCl(g), NaCl ↔ NaCl(g) and K_2CO_3 ↔ K_2CO_3(g) has been calculated based on Gibbs free energy minimization and compared. The results show that KCl(g) has the highest partial pressure of 0.7% at 950 °C, as compared to 0.4% for NaCl(g) and zero for K_2CO_3(g). This and the fact that Na_2CO_3 cannot evaporate indicate that KCl is the most volatile component among the four alkalis. This may also explain why the enhancement of gasification is smaller for KCl, cf. section 4.3, as most of KCl has been evaporated and left the char early, and thus the catalytic effect on gasification is not strong.

4.5. Agglomerates and alkali distribution in particles

Partial bed agglomeration of the braunite was found during the series with K_2CO_3-fuel, Na_2CO_3-fuel, KCl-fuel or NaCl-fuel, as seen in Fig. 6. The bulk bed material in the container has non-agglomerated particles as the major part, while a small amount of particles stuck together and formed agglomerates as indicated by the pencil tip. These agglomerates have a size of 2–5 mm as a result of particles combination, and they are very easy to break up with fingers. Because of this and only a small part
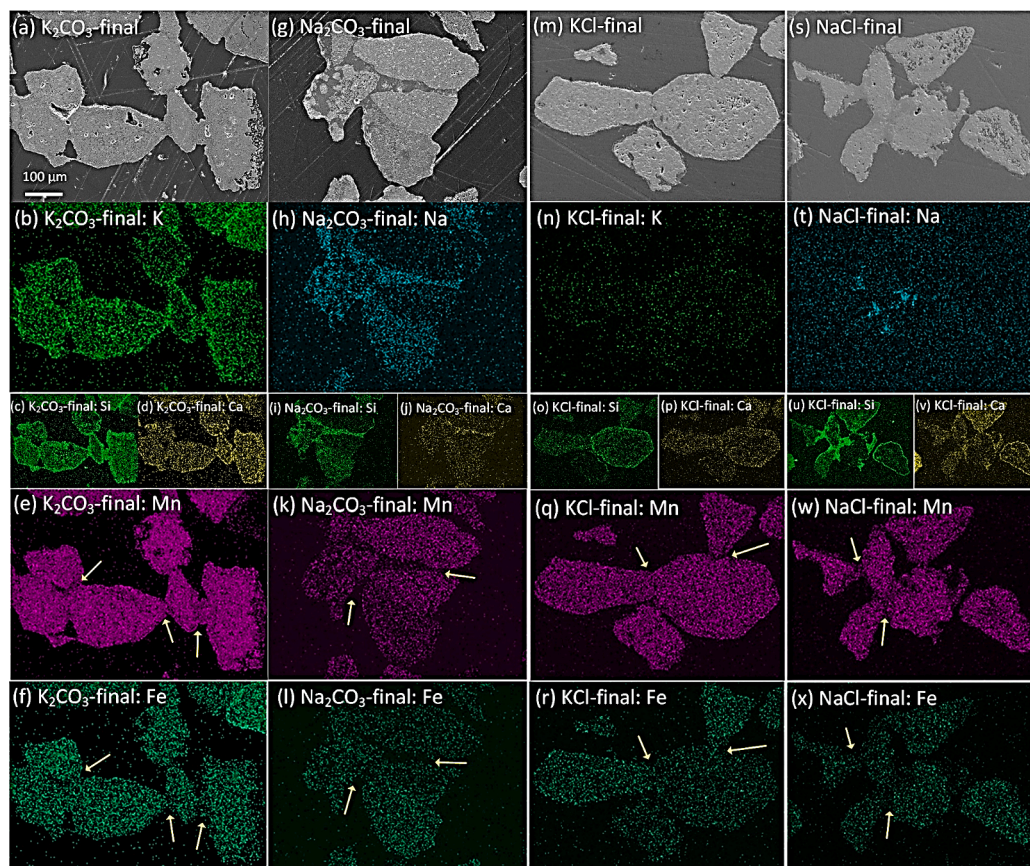

Fig. 7. SEM-EDX element mapping analyses of the cross-section of agglomerates from the bed material after final cycles with alkali-fuel samples: (a-f) used with K_2CO_3-fuel, (g-l) used with Na_2CO_3-fuel, (m-r) used with KCl-fuel and (s-x) used with NaCl-fuel. Yellow arrow shows the bridge positions between particles. Data for K_2CO_3-fuel and Na_2CO_3-fuel are from previous work [28]. (For interpretation of the references to colour in this figure legend, the reader is referred to the web version of this article.)
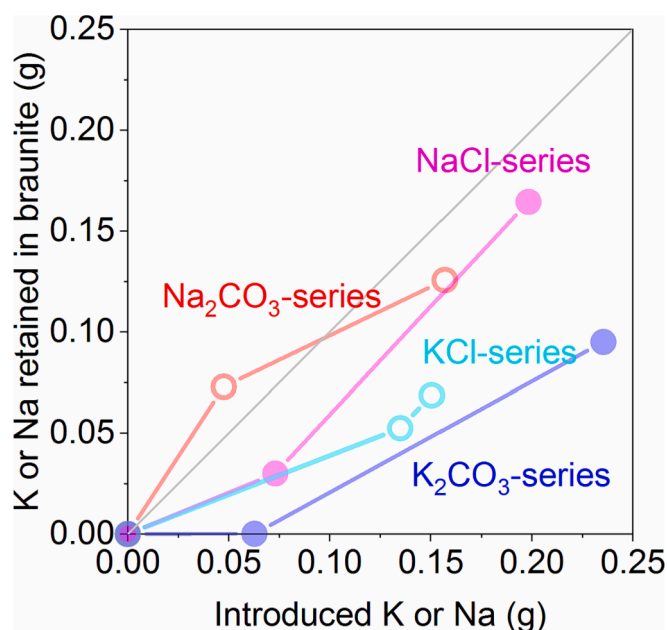
Fig. 8. Retention of K and Na in the braunite as a function of cumulative amount of K and Na introduced. K$_2$CO$_3$ and Na$_2$CO$_3$ data are from previous work [28].

of the bed being agglomerated, the agglomerations are denoted as partial agglomerations. At the same time many pressure measurements suggest that the beds are not properly fluidized, i.e. agglomerated. It can be speculated that there is a reversible agglomeration phenomena that more or less disappears when temperature is lowered. There are occasional experiences from CLC pilot operation where particles have been stuck in the cyclone, blocking circulation, and then, when temperature is lowered, the particles start to flow freely again with no remaining effects. The partial agglomeration phenomenon could be an explanation for the fluctuation increase after bed sampling from middle cycles, as observed in Fig. 5.

Fig. 7 further shows examples of partial agglomeration and the resulting bridges between particles through SEM-EDX mapping of the sample cross-sections. The SEM-EDX of K$_2$CO$_3$-final and Na$_2$CO$_3$-final cross-sections shows clear accumulation of K and Na in the bridges between particles (Fig. 7b and h), whereas for the KCl-final and NaCl-final samples, alkali accumulation is not clearly seen. Interestingly, the distribution of Mn and Fe in the bridges of Na$_2$CO$_3$-final is quite different to those of the other three samples. In the case of Na$_2$CO$_3$-final (Fig. 7k and l), the bridges are dark which means that there is no Mn and Fe in the bridge. Thus, the bridges of Na$_2$CO$_3$-final sample have no coexistence of Na, Mn and Fe. On the contrary, Mn and Fe are present in the bridges of K$_2$CO$_3$-final, KCl-final and NaCl-final samples, and coexistance of alkali, Mn and Fe is seen for these three samples. This might suggest different mechanisms of agglomerate formation for the latter three cases as compared to Na$_2$CO$_3$. Presumably, alkalis in K$_2$CO$_3$-fuel, KCl-fuel and NaCl-fuel interacted with Mn and Fe, and this resulted in low-melting point compounds [49] (e.g. K-Mn-Fe or Na-Mn-Fe system), which melted and stuck particles together to form agglomerates [28]. However, in the case of the Na$_2$CO$_3$ series, Mn and Fe do not seem to participate in the formation of agglomerates. The agglomeration with Na$_2$CO$_3$-fuel could be solely driven by the gluing of particles through the sticky layers formed by Ca-Si-Na systems [28,50,51]. Therefore, the resulting sticky layer sticks smaller oxygen carrier particles and this gradually forms agglomerates. More details of the two mechanisms is described in previous work [28].

Table 4
The amount of alkalis introduced and retained in the oxygen carrier.

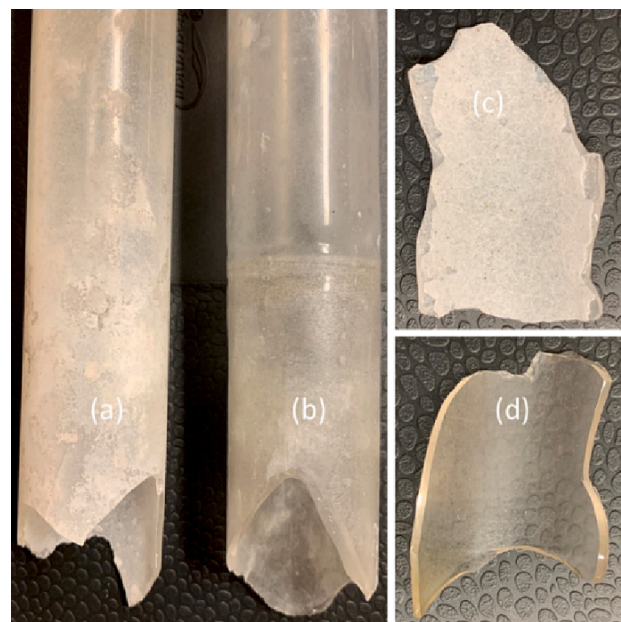|	K from K$_2$CO$_3$	Na from Na$_2$CO$_3$	K from KCl	Na from NaCl
Added (g)	0.235	0.157	0.151	0.198
Added (mol)	0.00604	0.00683	0.00386	0.00862
Retention (g)	0.095	0.126	0.0686	0.164
Retention (mol)	0.00243	0.00546	0.00176	0.00715
Retention/Added (%)	40.4	80.3	45.4	82.8

Fig. 9. Comparison between broken reactor tube, and tube pieces, of the quartz reactor from after KCl series (a, c) and after normal operation (b, d).

4.6. Alkali retention in the bed and interaction with the reactor

In Fig. 8, the amount of K and Na measured in the middle and final braunite samples are compared with the cumulative addition. Total added K and Na with K$_2$CO$_3$-fuel, Na$_2$CO$_3$-fuel, KCl-fuel and NaCl-fuel was 0.16, 0.24, 0.15 and 0.20 g which is 0.75–1.2% of the braunite weight. The Na retention increased quickly as more sodium was added, and more than 80% of the Na introduced with Na$_2$CO$_3$ and NaCl were finally found in the braunite. In the case of K$_2$CO$_3$-charcoal and KCl-charcoal, around 40% of K was retained. This indicates that potassium has a higher affinity towards the retention in the oxygen carrier, as compared to sodium. The amount of alkalis introduced and retained is also presented in Table 4. The retention of K and Na is also seen above in the SEM-EDX results, where the alkalis are found in the used oxygen carrier. However, the data does not allow any safe conclusions when comparing the chlorides with the carbonates.

In addition to the interaction with bed material, the KCl also reacted with the inner wall of the quartz reactor, as shown in Fig. 9. A thick, yellowish and shell-like layer (in Fig. 9a and c), which covered the inner wall, was formed after the 42 cycles in the KCl-charcoal series. This is absent for the reactor when used for normal experiments without alkali presence, see Fig. 9b and d. The layer in Fig. 9a and c seems to be the result of strong alkali corrosion of the inner wall, so the wall was gradually "eaten" by the alkali. As discussed in section 4.4 above, the high volatility and the fast evaporation [47] of KCl might be responsible for the severe wall corrosion. The reactor wall after the KCl-fuel series was thin and fragile and was easily broken down. The quartz reactor broke during the cooling down process, it happened at around 400–500
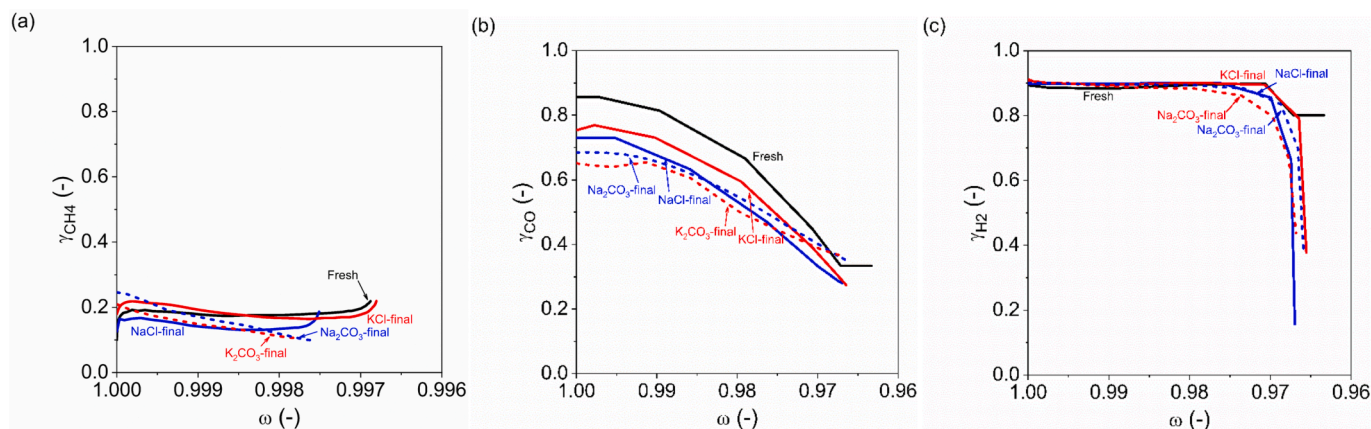
Fig. 10. Comparison of gas yield from each gas component (a) CH$_4$, (b) CO and (c) H$_2$. The data for K$_2$CO$_3$-final and Na$_2$CO$_3$-final is from previous work [28].

°C. Fig. 9a and c show pieces of the broken reactor after the cycle 42 in the KCl series experiments. For the other alkalis (NaCl, K$_2$CO$_3$, Na$_2$CO$_3$), some interaction with the quartz wall was also noticed, but the effects were far less severe than.

A relevant question is the influence of the alkali interaction with walls on the test results. However, the surface area of the particles in the bed is more than two orders of magnitude greater than that of the surrounding wall. Thus, the effect of the walls on the experiments is likely negligible except for putting an end to the KCl test series.

4.7. Evolution of braunite reactivity

The fresh and used oxygen carrier samples were tested with CH$_4$ and syngas to evaluate the reactivity with CH$_4$, CO and H$_2$. The gas yield is used to compare the reactivity between the fresh and used samples as seen in Fig. 10. In the case of reacting with CH$_4$, the gas yield for all the oxygen carriers is similar (0.1–0.25), but a little higher reactivity is noticed for the fresh oxygen carrier. Regarding the reactivity with CO, the gas yield is in the range of 0.27–0.86 and decreases as oxygen in the oxygen carrier is consumed. The fresh braunite has the highest reactivity, followed by KCl-final, whereas the others have somewhat lower reactivity. In the case with H$_2$, the estimated gas yield is stable at 0.9 during most of the whole cycle for all the five samples. It is known that H$_2$ is normally very reactive to most oxygen carriers and a full conversion would not be unexpected. In fact, it is very unlikely that the actual conversion would be stable at 0.9 through most of the period for all the samples. It can be added that the on-line analysis of hydrogen is somewhat complex, as it is based on heat conductivity of the gas and the conductivity varies between the different gases. Therefore, the gas analyzer performs a compensation for the concentrations of other gases. Most likely, the conversion of hydrogen was essentially complete and the deviation from one an artifact. Thus, H$_2$ has the highest reactivity, CO has a medium reactivity while CH$_4$ is the least reactive with the manganese ore. The conversion of CO and H$_2$ is high considering the low mass to flow ratio in the syngas tests, which corresponds to 23 kg oxygen carrier per MW.

5. Conclusions

The interaction between two alkali salts, KCl and NaCl, and a Mn ore oxygen carrier has been investigated in using batch fluidized bed experiments and various characterizations. The results have been compared to previous results for K$_2$CO$_3$ and Na$_2$CO$_3$ with the same Mn ore oxygen carrier. The following conclusions can be drawn.

- The char gasification was enhanced by a factor of 3–4 in presence of KCl and NaCl, compared to 8–10 times when using K$_2$CO$_3$ and Na$_2$CO$_3$.
- The potassium salts, K$_2$CO$_3$ and KCl, causes earlier onset of agglomeration/defluidization as compared to sodium salts, Na$_2$CO$_3$ and K$_2$CO$_3$. Alkali chlorides showed less permanence of partial defluidization as compared to the carbonates.
- Fe and Mn may take part in reactions with Si and Ca in the braunite forming agglomerates in presence of K$_2$CO$_3$, KCl and NaCl series, whereas they do not seem to be involved in agglomerate formation in presenece of Na$_2$CO$_3$.
- 40% of the K and 80% of the Na added with the fuel was retained in the Mn ore bed material after the experiments.
- The reactivity of alkali-exposed oxygen carrier with CH$_4$ and H$_2$ is fairly similar to the fresh material, whereas the oxygen carrier reactivity with CO is lower after use with alkalis.

CRediT authorship contribution statement

Daofeng Mei: Conceptualization, Methodology, Investigation, Formal analysis, Data curation, Writing – original draft, Writing – review & editing, Visualization. **Anders Lyngfelt:** Conceptualization, Methodology, Resources, Writing – review & editing, Supervision, Project administration, Funding acquisition. **Henrik Leion:** Methodology, Resources, Data curation, Writing – review & editing, Supervision. **Tobias Mattisson:** Methodology, Resources, Writing – review & editing, Supervision, Project administration, Funding acquisition.

Declaration of Competing Interest

The authors declare that they have no known competing financial interests or personal relationships that could have appeared to influence the work reported in this paper.

Data availability

Data will be made available on request.

References

[1] Lewis WK, Gilliland ER. Production of pure carbon dioxide. US Patent. 2. 665-971. 1954.

[2] Lyngfelt A, Kronberger B, Adánez J, Morin J-X, and Hurst P. The GRACE project. Development of oxygen carrier particles for chemical-looping combustion. Design and operation of a 10 kW chemical-looping combustor. In 7th International Conference on Greenhouse Gas Control Technologies. Vancouver. (2004).

[3] Lyngfelt A, Thunman H. Construction and 100 h of operational experience of a 10-kW chemical-looping combustor. Carbon Dioxide Capture for Storage in Deep Geologic Formations–Results from the CO_2 Capture Project. 1. (2005). 625-645.

[4] Berguerand N, Lyngfelt A. Design and operation of a 10 kW_{th} chemical-looping combustor for solid fuels - Testing with South African coal. Fuel 2008;87:2713–26.

[5] Berguerand N, Lyngfelt A. The use of petroleum coke as fuel in a 10 kW_{th} chemical-looping combustor. Int J Greenhouse Gas Control 2008;2:169–79.

[6] Ishida M, Jin HG. A new advanced power-generation system using chemical-looping combustion. Energy 1994;9(4):415–22. https://doi.org/10.1016/0360-5442(94)90120-1.

[7] Ströhle J, Orth M, Epple B. Design and operation of a 1 MW_{th} chemical looping plant. Appl Energy 2014;113:1490–5. https://doi.org/10.1016/j.apenergy.2013.09.008.

[8] Adánez J, Abad A, Mendiara T, Gayán P, de Diego LF, García-Labiano F. Chemical looping combustion of solid fuels. Prog Energy Combust Sci 2018;65:6–66. https://doi.org/10.1016/j.pecs.2017.07.005.

[9] Chemical LA, Combustion L. Status and Development Challenges. Energ. Fuel 2020;34:9077–93. https://doi.org/10.1021/acs.energyfuels.0c01454.

[10] Matzen M, Pinkerton J, Wang X, Demirel Y. Use of natural ores as oxygen carriers in chemical looping combustion: A review. Int J Greenhouse Gas Control 2017;65:1–14. https://doi.org/10.1016/j.ijggc.2017.08.008.

[11] Mei D, Soleimanisalim AH, Linderholm C, Lyngfelt A, Mattisson T. Reactivity and lifetime assessment of an oxygen releasable manganese ore with biomass fuels in a 10 kW_{th} pilot rig for chemical looping combustion. Fuel Process Technol 2021;215:106743. https://doi.org/10.1016/j.fuproc.2021.106743.

[12] Mei D, Linderholm C, Lyngfelt A. Performance of an oxy-polishing step in the 100 kW_{th} chemical looping combustion prototype. Chem Eng J 2021;409:128202. https://doi.org/10.1016/j.cej.2020.128202.

[13] Linderholm C, Lyngfelt A, Rydén M., Schmitz M. Chemical-looping combustion of biomass in a 100 kW pilot. Proceedings of the 25th European Biomass Conference and Exhibition (EUBCE), June 12-15, Stockholm, Sweden. 2017. 412-5.

[14] Schmitz M, Linderholm C. Chemical looping combustion of biomass in 10 and 100 kW pilots - Analysis of conversion and lifetime using a sintered manganese ore. Fuel 2018;231:73–84. https://doi.org/10.1016/j.fuel.2018.05.071.

[15] Moldenhauer P, Linderholm C, Rydén M, Lyngfelt A. Avoiding CO_2 Capture Effort and Cost for Negative CO_2 Emissions using Industrial Waste in Chemical-Looping Combustion/Gasification of Biomass. Miti Adapt Strateg Glob Chang 2020;25:1–24. https://doi.org/10.1007/s11027-019-9843-2.

[16] Schmitz M, Linderholm C, Lyngfelt A. Operational Experience of CO_2 Capture Using Chemical-Looping Combustion of Biomass-based Fuels in a 100 kW Unit. 1st International Conference on Negative CO2 Emissions. Sweden: Gothenburg; 2018.

[17] Gogolev I, Linderholm C, Gall D, Schmitz M, Mattisson T, Pettersson JB, et al. Chemical-Looping Combustion in a 100 kW Unit Using a Mixture of Synthetic and Natural Oxygen Carriers - Operational Results and Fate of Biomass Fuel Alkali. Int J Greenhouse Gas Control 2019;88:371–82. https://doi.org/10.1016/j.ijggc.2019.06.020.

[18] Gogolev I, Pikkarainen T, Kauppinen J, Linderholm C, Steenari B-M, Lyngfelt A. Investigation of biomass alkali release in a dual circulating fluidized bed chemical looping combustion system. Fuel 2021;297:120743. https://doi.org/10.1016/j.fuel.2021.120743.

[19] Gogolev I, Soleimanisalim AH, Mei D, Lyngfelt A. Effects of Temperature, Operation Mode, and Steam Concentration on Alkali Release in Chemical Looping Conversion of Biomass – Experimental Investigation in a 10 kWth Pilot. Energy Fuel 2022;36:9551–70. https://doi.org/10.1021/acs.energyfuels.1c04353.

[20] Vilches TB, Lind F, Rydén M, Thunman H. Experience of more than 1000 h of operation with oxygen carriers and solid biomass at large scale. Appl Energy 2017; 190:1174–83. https://doi.org/10.1016/j.apenergy.2017.01.032.

[21] Zevenhoven M, Yrjas P, Skrifvars B-J, Hupa M. Characterization of Ash-Forming Matter in Various Solid Fuels by Selective Leaching and Its Implications for Fluidized-Bed Combustion. Energ Fuel 2012;26:6366–86. https://doi.org/10.1021/ef300621j.

[22] Di Giuliano A, Capone S, Anatone M, Gallucci K. Chemical Looping Combustion and Gasification: A Review and a Focus on European Research Projects. Ind Eng Chem Res 2022;61:14403–32. https://doi.org/10.1021/acs.iecr.2c02677.

[23] Goel A, Moghaddam EM, Liu W, He C, Konttinen J. Biomass chemical looping gasification for high-quality syngas: A critical review and technological outlooks. Energ Convers Manage 2022;268:116020. https://doi.org/10.1016/j.enconman.2022.116020.

[24] Scala F, Chirone R. An SEM/EDX study of bed agglomerates formed during fluidized bed combustion of three biomass fuels. Biomass Bioenergy 2008;32:252–66. https://doi.org/10.1016/j.biombioe.2007.09.009.

[25] Morris JD, Daood SS, Chilton S, Nimmo W. Mechanisms and mitigation of agglomeration during fluidized bed combustion of biomass: A review. Fuel 2018; 230:452–73. https://doi.org/10.1016/j.fuel.2018.04.098.

[26] Lyngfelt A, Leckner B. A 1000 MW_{th} boiler for chemical-looping combustion of solid fuels – Discussion of design and costs. Appl Energy 2015;157:475–87. https://doi.org/10.1016/j.apenergy.2015.04.057.

[27] Lyngfelt A, Pallarès D, Linderholm C, Lind F, Thunman H, Leckner B. Achieving Adequate Circulation in Chemical Looping Combustion—Design Proposal for a 200 MW_{th} Chemical Looping Combustion Circulating Fluidized Bed Boiler. Energy Fuel 2022;36:9588–615. https://doi.org/10.1021/acs.energyfuels.1c03615.

[28] Mei D, Lyngfelt A, Leion H, Linderholm C, Mattisson T. Oxygen carrier and alkali interaction in chemical looping combustion: case study using a braunite Mn ore and charcoal impregnated with K_2CO_3 or Na_2CO_3. Energy Fuel 2022;36(17): 9470–84. https://doi.org/10.1021/acs.energyfuels.2c00553.

[29] Rubel A, Zhang Y, Neathery JK, Liu K. Comparative Study of the Effect of Different Coal Fly Ashes on the Performance of Oxygen Carriers for Chemical Looping Combustion. Energy Fuel 2012;26:3156–61. https://doi.org/10.1021/ef201790m.

[30] Siriwardane R, Tian H, Richards G, Simonyi T, Poston J. Chemical-Looping Combustion of Coal with Metal Oxide Oxygen Carriers. Energy Fuel 2009;23: 3885–92. https://doi.org/10.1021/ef9001605.

[31] Gu H, Shen L, Zhong Z, Zhou Y, Liu W, Niu X, et al. Interaction between biomass ash and iron ore oxygen carrier during chemical looping combustion. Chem Eng J 2015;277:70–8. https://doi.org/10.1016/j.cej.2015.04.105.

[32] Lin Y, Wang H, Wang Y, Huo R, Huang Z, Liu M, et al. Review of Biomass Chemical Looping Gasification in China. Energy Fuel 2020;34:7847–62. https://doi.org/10.1021/acs.energyfuels.0c01022.

[33] Yin Ke, Wang H, Veksha A, Dou X, Khairunnisa Binte Mohamed D, Heberlein S, et al. Oxygen carriers from incineration bottom ash for chemical looping combustion of syngas: Effect of composition on combustion efficiency. Chem Eng J 2021;405:127068.

[34] Bao J, Li Z, Cai N. Promoting the Reduction Reactivity of Ilmenite by Introducing Foreign Ions in Chemical Looping Combustion. Ind Eng Chem Res 2013;52: 6119–28. https://doi.org/10.1021/ie400237p.

[35] Störner F, Hildor F, Leion H, Zevenhoven M, Hupa L, Rydén M. Potassium Ash Interactions with Oxygen Carriers Steel Converter Slag and Iron Mill Scale in Chemical-Looping Combustion of Biomass—Experimental Evaluation Using Model Compounds. Energy Fuel 2020;34:2304–14. https://doi.org/10.1021/acs.energyfuels.9b03616.

[36] Ilyushechkin AY, Kochanek M, Lim S. Interactions between oxygen carriers used for chemical looping combustion and ash from brown coals. Fuel Process Technol 2016;147:71–82. https://doi.org/10.1016/j.fuproc.2015.11.019.

[37] Chen L, Ge H, Li P, Sheng C, Song T. Biomass ash chemistry in chemical looping: Interaction between organic-K and Fe_2O_3/Al_2O_3 oxygen carrier using cellulose-CH_3COOK as model compound. Biomass Bioenergy 2022;163:106533. https://doi.org/10.1016/j.biombioe.2022.106533.

[38] Pikkarainen T, Hiltunen I. Chemical looping combustion of solid biomass – performance of ilmenite and braunite as oxygen carrier materials. Proceedings of the 25th European Biomass Conference and Exhibition (EUBCE), June 12-15, Stockholm, Sweden. 2017. 1837-44.

[39] Mei D, Lyngfelt A, Leion H, Mattisson T. Batch fluidized bed study of the interaction between alkali impurities and braunite oxygen carrier in chemical looping combustion. the 24th International Conference on Fluidized Bed Conversion. Gothenburg. 2022.

[40] Sundqvist S, Khalilian N, Leion H, Mattisson T, Lyngfelt A. Manganese ores as oxygen carriers for chemical-looping combustion (CLC) and chemical-looping with oxygen uncoupling (CLOU). J Environ Chem Eng 2017;5:2552–63. https://doi.org/10.1016/j.jece.2017.05.007.

[41] Leion H, Frick V, Hildor F. Experimental Method and Setup for Laboratory Fluidized Bed Reactor Testing. Energies 2018;11:2505. https://doi.org/10.3390/en11102505.

[42] Mei D, Soleimanisalim AH, Lyngfelt A, Leion H, Linderholm C, Mattisson T. Modelling of gas conversion with an analytical reactor model for biomass chemical looping combustion (bio-CLC) of solid fuels. Chem Eng J 2022;433:133563.

[43] McKee DW. Gasification of graphite in carbon dioxide and water vapor—the catalytic effects of alkali metal salts. Carbon 1982;20(1):59–66. https://doi.org/10.1016/0008-6223(82)90075-6.

[44] Śpiewak K, Czerski G, Porada S. Effect of K, Na and Ca-based catalysts on the steam gasification reactions of coal. Part I: Type and amount of one-component catalysts. Chem Eng Sci 2021;229:116024.

[45] Hüttinger KJ, Minges R. The influence of the catalyst precursor anion in catalysis of water vapour gasification of carbon by potassium. Fuel 1986;65(8):1122–8.

[46] Liu T, Mao L, Jiao F, Wu C, Zheng M, Li H. Catalytic performance of Na/Ca-based fluxes for coal char gasification. Green Process Synth 2022;11:204–17. https://doi.org/10.1515/gps-2022-0020.

[47] Li X, He F, Su X, Behrendt F, Gao Z, Wang H. Evaporation rate of potassium chloride in combustion of herbaceous biomass and its calculation. Fuel 2019;257: 116021. https://doi.org/10.1016/j.fuel.2019.116021.

[48] Zhao H, Song Q, Wu X, Yao Q. Study on the Transformation of Inherent Potassium during the Fast-Pyrolysis Process of Rice Straw. Energy Fuels 2015;29(10): 6404–11. https://doi.org/10.1021/acs.energyfuels.5b00851.

[49] Boström D, Skoglund N, Grimm A, Boman C, Öhman M, Broström M, et al. Ash transformation chemistry during combustion of biomass. Energy Fuels 2012;26: 85–93. https://doi.org/10.1021/ef201205b.

[50] Niu Y, Tan H, Hui S. Ash-related issues during biomass combustion: Alkali-induced slagging, silicate melt-induced slagging (ash fusion), agglomeration, corrosion, ash utilization, and related countermeasures. Prog Energy Combust Sci 2016;52:1–61. https://doi.org/10.1016/j.pecs.2015.09.003.

[51] Grimm A, Öhman M, Lindberg T, Fredriksson A, Boström D. Bed Agglomeration Characteristics in Fluidized-Bed Combustion of Biomass Fuels Using Olivine as Bed Material. Energy Fuels 2012;26(7):4550–9. https://doi.org/10.1021/ef300569n.